Published in small NANO MICRO

3D printing of highly conductive nanocomposites for the functional optimization of liquid sensors

By *Kambiz Chizari, Mohamed Amine Daoud, Anil Raj Ravindran and Daniel Therriault**

[*] Prof. D. Therriault

Laboratory for Multiscale Mechanics (LM2), Center for applied research on polymers (CREPEC), Department of Mechanical Engineering, Polytechnique Montréal, Montréal, QC H3C 3A7, CANADA.
Email: daniel.therriault@polymtl.ca

Conductive nanocomposites (CNCs) have shown promising electrical properties useful for various applications such as sensors,[1, 2] electronics,[3-6] electromagnetic interference (EMI) shielding[7, 8] and lightning strike protection in airplanes.[9, 10] CNCs were used for fabrication of different types of sensors such as biosensors,[11, 12] gas sensors, [13, 14] strain sensors [15-18] and liquid sensors.[19, 20] These sensors function usually based on the electrical conductivity alteration of CNCs sensors when they enter in contact with certain materials or when their structure become stretched/compressed due to applied strain/stress. Stretching the CNCs can increase the distance between conductive nanofillers and decrease the number of percolation pathways which leads to a decrease in their conductivity.[2, 15, 16, 18, 21] The conductivity of the CNC used for liquid sensors varies when it enters in contact with a liquid due to the swelling phenomenon.[19] The liquid entering in the structure of polymer matrix, expands its structure and elongate the distance between conductive nanofillers. Liquid sensors can be useful for sensing the concentration of methanol in fuel cells[22] and detecting the leakage of organic solvents which can be applied for security control for pipelines, refineries, gas stations and in automobiles.[19, 20] The sensitivity of

carbon nanotube (CNT)/polylactic acid (PLA) liquid sensors to different liquids such as dichloromethane (DCM), Tetrahydrofuran (THF), chloroform, toluene, methanol, ethanol, n-hexane, acetone and ethyl acetate were previously reported.[19, 20, 23, 24] A comparison of the liquid sensor sensitivity to these tested liquids showed their higher sensitivity for DCM, THF and acetone.

Conventional methods used for forming CNCs (e.g., solvent casting, compression molding or injection molding) usually require the utilization of molds while 3D printing (3DP) methods build forms from a digitally designed 3D models.[25] 3DP enables us to fabricate configuration with different structural parameters without the need to make a mold for each structure. This feature of 3DP make this method one of the most promising fabrication methods suitable for experimental studying of the topology optimizations. An investigation of the mechanical behavior of synthetic elastomeric webs as a function of their architectural features using 3DP is recently reported.[26]

Many different types of 3D printing methods (e.g., fused deposition modeling (FDM),[25, 27, 28] selective laser sintering (SLS),[29] stereolithography,[30, 31] solvent cast 3DP (SC3DP)[32] and UV assisted 3DP (UV3DP))[33, 34] have been developed so far. 3D printing of conductive materials has been always a challenge since the most frequently used conductive materials are metals. Due to their high melting temperature, their utilization as an ink for 3DP methods dealing with melting and extruding the material from a nozzle (i.e., FDM) is challenging. M.D. Dickey and his co-workers have reported direct-write 3D printing of metallic structures by extrusion of liquid metal from a nozzle.[35] SLS has been used for fabrication of metallic structures by sintering of metal powder using heating

originated from a laser beam.[36] Other efforts have been done on printing of conductive polymer based nanocomposites using FDM,[37] SC3DP[23, 38, 39] and UV3DP.[17] Conductive structures with electrical conductivity of ~ 10 S/m were made by FDM method using a carbon black/polycaprolactone composite ink. [37] Since SC3DP and UV3DP can function at room temperature, they do not deal with the problems originated from the variation in melting point and viscosity due to the adding of fillers in the original polymer. Printing of conductive nanocomposites with electrical conductivity of ~ 100 S/m was reported for CNT/PLA ink. [39] Scaffolds from graphene based material with electrical conductivity of 278 S/m were fabricated using 3D printing method suitable for printing of aerogels.[40]

Here we report the fabrication of highly conductive CNTs/PLA nanocomposites used as 3D printable conductive inks for fabrication of conductive scaffold structures applicable as liquid sensors. 3D printing enables us to control the structural parameters of liquid sensors and study their influence on the sensitivity of the obtained liquid sensor which can be useful for structures made from repeated patterns of filaments, such as for liquid sensors in form of textiles.[24] This work shows how 3DP can be used to explore experimentally the topology optimization of sensors where their sensitivity is related to their structural parameters.

The process of fabrication and testing of liquid sensors are illustrated in **Figure 1.** Ball mill mixing method enabled us to fabricate CNT/PLA composites with very high CNTs concentration (i.e., up to 40 wt.%) with high electrical conductivities up to about 3800 S/m). Structures in form of scaffolds with different structural parameters (i.e., filament diameter, inter-filament spacing (IFS), thickness of scaffolds and configuration patterns)

were fabricated using solvent-cast 3D printing method. The filament diameters were varied from 128 μm to 432 μm by changing the extrusion nozzle used for 3D printing within the range of 100 to 330 μm. IFS, number of printed layers and the printed patterns were controlled by modifying a computer aided design (CAD) software. Figure 1d shows SEM images of different printed patterns denoted as I: open window, II: closed window, III: Zigzag I and IV: Zigzag II. The thickness of the scaffolds varied from 0.17 to 1.11 mm by changing the number of printed layers from 2 to 10. Figure 1e shows a schematic and an optical photo of the U shaped cut of the scaffolds used for the liquid sensitivity measurements. They were cut in U shape to have a specific part of the sample immersed in the liquid while the electrodes were connected to the top extremities without contacting with the liquid. A typical graph of relative resistance change (RRC) resulted from an immersion/drying cycle of a scaffold printed with a 200 μm inner diameter nozzle in four layers with IFS of 0.7 mm is shown in Figure 1f. The immersion/drying time was at 120/600 s. RRC of the liquid sensor increased while it was immersed in the liquid due to the polymer swelling originated from the diffusion of liquid inside the polymer matrix. RRC decreased gradually when the scaffold was taken out of the liquid. At this time although the scaffold is out of liquid, due to the capillary forces of grid-like structure, it can keep a portion of the liquid inside its structure which slow down the RRC decreasing rate. After about 400 s when the liquid is evaporated and left the structure, the RRC decreased with a faster rate to the initial resistivity. Seven immersion/drying cycles were tested for each sample and the average RRC of the last four cycles, where the liquid

sensitivity becomes more stable, were used to compare the sensitivity of liquid sensors with different configurations.

The influence of four different structural parameters (i.e., IFS, scaffold thickness, filament diameter and structural patterns) on the sensitivity of the printed scaffold liquid sensors was investigated and the results are shown in **Figure 2**. Figure 2a demonstrates the effect of IFS on the sensitivity of the liquid sensors printed in four layers with a nozzle diameter of 200 µm. The average RRC varied from ~78% to ~238% by changing the IFS in the range of 0.2 to 1.9 mm. The lowest liquid sensitivity (i.e., 78%) was related to the scaffold with the lowest IFS which can be considered as the most compact structure. The number of filaments along the length and width of the scaffolds increases by decreasing the IFS leading to more intersections of the top and bottom neighbouring filament layers. The surfaces covered in these intersections are hardly accessible to the liquid and increasing the inaccessible surface area decreases the effect of liquid on the RRC of the liquid sensors. The optimum liquid sensitivity was observed for the scaffolds with IFS in the range of 0.5 to 1.5 where the RRC varied between 124 to 238 %. The slight decrease in the sensitivity of the liquid sensors (at 118 %) for the liquid sensor with IFS of 1.9 mm can be related to the fact that at higher IFS the scaffolds are less dense and less material contacts the liquid which lowers the total conductivity and the detection of its variation. Figure 2b shows the influence of the filament diameter on the sensitivity of the liquid sensor printed in four layers and IFS of~ 0.7 mm. The highest RRC (i.e., 290 %) was obtained at the lowest filament diameter (i.e., 128 µm). This value decreased gradually to 58 % by increasing the filament diameter up to 433 µm. The decrease of the liquid

sensitivity by increasing the filament diameters might be due to the difference in the liquid diffusion time for the swelling of the filaments. Kobashi et al. have tested liquid sensors in form of a U shaped bulk solid CNT/PLA with different thicknesses in the range of 0.1 to 0.5 mm and reported a sharper response and faster recovery of the composite electrical resistance during immersion/drying cycles for thinner liquid sensors.[19] In the case of scaffold, since the diffusion pathway is longer for larger filament diameters, the liquid requires more time to fill and expand the PLA matrix which leads to lower sensitivity of the liquid sensor. Figure 2c demonstrates the variation of the RRC as a function of scaffold thicknesses for the scaffolds printed by a nozzle diameter of 200 μm and IFS of ~0.7 mm. Increasing in the scaffold thickness from 0.17 to 1.11 mm led to a decrease in RRC from 196 to as low as 19 %. Since the distance between the printed layers are small (e.g., < 100 μm), a slight deformation before the total evaporation of DCM, the ink's volatile solvent, during the printing process can cause partial overlapping of these filaments. Increasing the number of printed layers increases the area of these covered surfaces and since the testing liquid has less access to the covered areas, lower sensitivity can be obtained for scaffold liquid sensors with higher number of printed layers. The liquid sensitivities of the liquid sensors printed in different patterns are demonstrated in Figure 2d. The relative resistance change of the liquid sensors in different scaffold patterns varied between 93 to 188 %. Considering the fact that the variation of the relative resistance change for the open window patterns fabricated with similar printing parameters (i.e., IFS: ~ 0.7, number of layers: 4 and nozzle inner diameter: 200 μm) varied between 123 to 180% (Figure 2a), the effect of pattern variation on the liquid sensitivity was relatively low.

Based on these results the overall optimum structural parameters of a CNT/PLA grid like liquid sensor can be considered for scaffold structure with filament diameter <250 μm, thickness <0.6 mm and IFS between 0.5 to 1.5 mm. The effects of filament diameter and scaffold thickness in the tested ranges are more remarkable compared to the influence of IFS and scaffold pattern on the sensitivity of the liquid sensors.

Figure 3a demonstrates the graph of RRC resulted from an immersion/drying cycle for the scaffolds with three representative IFSs (i.e., 0.2, 1.28 and 1.9 mm). The width of the peaks varied for different IFSs with a shortest width belonging to the scaffold with highest IFS and widest peak to the lowest IFS. The width of the peaks can be related to the liquid trapping in the structure since it can elongate the evaporation or escaping of the liquid from the liquid sensor. The effect of liquid trapping on the liquid sensitivity behaviour of CNT/PLA was previously reported for two different morphologies of helical and straight line shapes.[23] Increasing the duration of the liquid effect on the resistance change of the liquid sensor can be favourable for maintaining the leakage detection for a longer time. The influence of some of structural parameters (i.e., IFS, thickness and printed patterns) on the liquid trapping is investigated and showed in Figure 3b-e. The amount of trapped liquid is defined by the mass of liquid absorbed in the structure after the immersion and escaped the structure during the drying time which is named as liquid trapping. Figure 3b demonstrates the amount of liquid trapping for scaffolds with different IFSs. The general trend of the IFS effect on the liquid trapping is a decrease of the amount of trapped liquid by increasing the IFS. For the IFSs ranging between 0.2 to 0.68 mm the trapping liquid value varied between 0.2 to 0.4 g.s and it decreased to 0.04 g.s by raising the IFS to 1.9 mm. This trend

can be originated from the capillary forces that help to maintain higher mass of liquid for longer time before its evaporation when the pore sizes are smaller. For the scaffolds with higher IFS (e.g., 1.9 mm) due to lower capillary forces the liquid can drop and leave the structure which decreases the liquid effect during drying time. The optical photos of the scaffolds with two different IFS (i.e., 0.2 and 1.26 mm) immersed in a fluorescent solvent as a function of drying time is shown in Figure 3c. No obvious change of the trapped liquid in scaffold with IFS of 0.2 mm was observed during the first 20 s of drying time while in the case of scaffold with IFS of 1.26, some portion of liquid left the structure in the same drying duration. Based on these photos after 10 minutes of drying, > 70 % and < 30 % of the liquid was remained in the scaffolds with IFS of 0.2 and 1.26 mm, respectively. The influence of scaffolds thickness on their liquid sensitivity is displayed in Figure 3d. Decreasing the scaffold thickness led to a decrease in the mass of trapped liquid. Reducing the scaffold thicknesses leads to lower vacant volume which limits the amount of trapped liquid. Higher surface to volume ratio of the trapped liquid in thinner scaffolds can also cause its faster evaporation. Scaffold printed in 10 layers with a thickness of 1.11 mm could entrap acetone for about 12 times more than two layer scaffold with a thickness of about 0.17 mm. No significant difference in the quantity of trapped liquid was observed for scaffolds printed in different patterns with similar IFSs and number of layers (Figure 3e). These results shows that the amount of liquid entered and trapped in the structure depended more on the dimensional parameters such as IFS and thickness of scaffolds rather than the printed patterns.

Materials with low conductivities require higher applied voltage to function as a conductive material in electrical devices. Although the conductivity of CNT/PLA with 2 wt.% of carbon nanotubes (i.e., ~45 S/m) was sufficient enough for the investigation of the structural parameter effects on the sensitivity of the liquid sensors, composites with higher conductivities are required for their practical application using low applied voltages. CNT/PLA scaffolds with CNT concentration up to 30 wt.% and electrical conductivity up to ~ 2350 S/m were printed using solvent cast 3D printing method. A comparison of the electrical conductivity of the fabricated inks to other reported polymer based conductive composites suitable for 3D printing (e.g., <100 S/m[39], <1 S/m [41] and ~ 10 S/m[37]) demonstrates its high conductivity. SC3DP method enabled us to use CNT/PLA with high concentration of CNT since in this method the viscosity of the ink could be adjusted by varying the concentration of ink's solvent.[42] One of the main disadvantage of materials with low conductivity for applications that requires the electrical current variation detection, is that at low applied voltages the current is extremely low that its detection is impossible. The high conductivity of the printed scaffolds allowed us to perform the liquid sensitivity tests by using an applied voltage as low as 1.5 V. The results of the liquid sensitivity tests together with the conductivity of the bulk CNT/PLA nanocomposites are shown in **Figure 4**. The results showed an increasing trend of liquid sensitivity by raising the CNTs concentration in PLA. The RRC of liquid sensors could raise as high as ~ 78 % for the scaffolds made from CNT/PLA with CNT concentration of 30 wt.%. This increase can be related to the better detection of the variation in the resistivity at low applied voltage

(i.e., 1.5 V) of the CNT/PLA with higher percentages of CNTs due to their higher electrical conductivity.

In summary, various scaffold structures were made from CNT/PLA conductive composites using the solvent-cast 3D printing method. 3D printing enabled us to study the influence of different structural parameters (i.e., IFS, filament diameter, scaffold thickness and printing patterns) on the sensitivity of liquid sensors. .The sensitivity of the liquid sensors decreased by increasing the filament diameter and/or the thickness of the fabricated scaffolds. The liquid trapping tests showed that the amount of liquid trapped in the scaffold structures increased by decreasing the IFS and/or increasing the number of printed layers. Highly conductive CNT/PLA composite inks suitable for solvent-cast 3D printing method were fabricated by increasing the CNT concentration to 30 wt.%. The conductivity of these polymer based inks could reach up to ~2350 S/m which led to fabrication of liquid sensors that can show RRC of about 78 % using low applied voltage (i.e., 1.5 V).

This work demonstrates the utilization of the 3D printing method for the structural optimization of a conductive composite device. This technology can be used for structural optimization of configurations suitable for various applications such as different types of sensors (e.g., gas or strain sensors) and EMI shielding. Structural optimization using 3D printing method can facilitate complex topology optimizations using theoretical modelings where the required functionality is depended on various structural parameters. Printing highly conductive material in 3D can also be valuable for fabrication of complex conductive structures, useful for electronics in 3D circuits. Manipulating the electrical properties of printable conductive polymer based composites can lead to 3D printing of

different electrical components (e.g., resistance, capacitors and conductive interconnections).

Experimental Section

*Fabrication of nanocomposites***:** Carbon nanotubes (Nanocyl NC7000) were dispersed in the PLA (PLA 4032D, Natureworks LLC) via a ball mill mixing method (SPEX SamplePrep 8000M Mixer/Mill).[43] PLA/DCM with PLA concentration of 10 wt.% was placed inside a ball mill vial together with the required amount of CNTs (depending on the desired wt.% of CNT/PLA) and ball milled for 30 minutes. After the mixing, the material was taken out of ball mill vial and dried at room temperature for 24 hours.

3D printing of scaffolds: The obtained CNT/PLA nanocomposites were dissolved in DCM with a concentration of 30 wt.% to form an ink compatible for SC-3DP.[44] The ink was fed to a syringe which was then placed inside a syringe chamber of dispensing robot (Fisnar I&J2200-4). The extrusion pressure was controlled by a pressure regulator (HP-7X, EFD) set in range of 300 - 600 kPa in order to match the displacement rate of the robot ranging from 0.3 to 1 mm/sec. The selected values of the applied pressure and displacement of the nozzle depended on the concentration of CNTs and the viscosity of the prepared ink. The syringes and micro-needles ranging from 100 µm to 330 µm were supplied by Nordson EFD Company.

Conductivity measurements: The conductivity measurements were performed using four-point probe method. Five measurements were done on different parts of hot pressed CNT/PLA composites with dimensions of 12 × 102 × 0.6 mm. The applied electrical current varied from 1 to 5 mA using Keithley 6221 current source and the voltage was

measured on the samples in a distance of 25.4 mm by Keithley 2182A nanovoltmeter. The error bars are the standard deviation resulted from the five conductivity measurements. The volume conductivity was calculated from the resistance values resulted from the 4 point measurement considering the length and cross section area of the composite samples measured using a digital caliper (Lyman electronic digital caliper).

Liquid sensitivity tests. The liquid sensitivity of liquid sensors with a scaffold configuration was tested by measuring their electrical resistivity during immersion/drying cycles. Acetone was used as the testing solvent. Scaffolds were cut in U shape using a metallic blade. The bottom part of U-shaped was placed in the solvent and the electrodes of the resistivity meter were attached to the upper extremities. The Liquid sensors were immersed inside acetone and their electrical resistivity were tracked using a resistance meter (Keithley 6517B) connected to a PC and a Labview software. Seven immersion/drying cycles were done on each sample and the average value of the last four peaks was used to calculate the RRC and their error bars. The RRC is the percentage of the difference between the actual resistance and the initial resistance to the initial resistance of the liquid sensors. The immersion and drying times were set at 120 s and 600 s, respectively.

Liquid trapping tests: To measure the amount of liquid trapped in the structure of the scaffolds, the scaffolds in U shape were hanged to a hook under a digital scale (A&D GH-200). The mass of absorbed liquid was measured during the drying time after they were immersed in acetone (see Figure S2). This measurement repeated for five cycles with the immersion/drying time of 20/180 seconds. The values of the liquid trapping were

calculated from the integral of the curves of mass of absorbed liquid as a function of drying time.

Acknowledgements

The authors acknowledge the financial support from Natural Sciences and Engineering Research Council of Canada (NSERC). We would like to thank Prof. Frédéric Sirois and Martin Gagné from École Polytechnique de Montréal for providing us technical assistance with the electrical conductivity measurements. We also thank Dr. Shuang-Zhuang Guo for his technical assistance with the liquid sensitivity measurements and analyses.

References

1. Kang, X.; Mai, Z.; Zou, X.; Cai, P.; Mo, J., *Analytical Biochemistry* **2007,** *363* (1), 143-150.
2. Inpil, K.; Mark, J. S.; Jay, H. K.; Vesselin, S.; Donglu, S., *Smart Materials and Structures* **2006,** *15* (3), 737.
3. Bae, S.; Kim, H.; Lee, Y.; Xu, X.; Park, J.-S.; Zheng, Y.; Balakrishnan, J.; Lei, T.; Ri Kim, H.; Song, Y. I.; Kim, Y.-J.; Kim, K. S.; Ozyilmaz, B.; Ahn, J.-H.; Hong, B. H.; Iijima, S., *Nat Nano* **2010,** *5* (8), 574-578.
4. Eda, G.; Chhowalla, M., *Nano Letters* **2009,** *9* (2), 814-818.
5. Stankovich, S.; Dikin, D. A.; Dommett, G. H. B.; Kohlhaas, K. M.; Zimney, E. J.; Stach, E. A.; Piner, R. D.; Nguyen, S. T.; Ruoff, R. S., *Nature* **2006,** *442* (7100), 282-286.
6. Rogers, J. A.; Someya, T.; Huang, Y., *Science* **2010,** *327* (5973), 1603-1607.
7. Li, N.; Huang, Y.; Du, F.; He, X.; Lin, X.; Gao, H.; Ma, Y.; Li, F.; Chen, Y.; Eklund, P. C., *Nano Letters* **2006,** *6* (6), 1141-1145.
8. Arjmand, M.; Mahmoodi, M.; Gelves, G. A.; Park, S.; Sundararaj, U., *Carbon* **2011,** *49* (11), 3430-3440.
9. Gagné, M.; Therriault, D., *Progress in Aerospace Sciences* **2014,** *64*, 1-16.
10. Glatkowski, P. J.; Landis, D. H.; Piche, J. W.; Conroy, J. L., Carbon nanotube fiber-reinforced composite structures for EM and lightning strike protection. Google Patents: **2006**.

11. Wang, J.; Musameh, M., *Analytical Chemistry* **2003,** *75* (9), 2075-2079.
12. Wang, J., *Electroanalysis* **2005,** *17* (1), 7-14.
13. An, K. H.; Jeong, S. Y.; Hwang, H. R.; Lee, Y. H., *Advanced Materials* **2004,** *16* (12), 1005-1009.
14. Ong, K. G.; Zeng, K.; Grimes, C. A., *Sensors Journal, IEEE* **2002,** *2* (2), 82-88.
15. Hu, N.; Karube, Y.; Arai, M.; Watanabe, T.; Yan, C.; Li, Y.; Liu, Y.; Fukunaga, H., *Carbon* **2010,** *48* (3), 680-687.
16. Thostenson, E. T.; Chou, T. W., *Advanced Materials* **2006,** *18* (21), 2837-2841.
17. Farahani, R. D.; Dalir, H.; Le Borgne, V.; Gautier, L. A.; El Khakani, M. A.; Lévesque, M.; Therriault, D., *Nanotechnology* **2012,** *23* (8), 085502.
18. Yamada, T.; Hayamizu, Y.; Yamamoto, Y.; Yomogida, Y.; Izadi-Najafabadi, A.; Futaba, D. N.; Hata, K., *Nat Nano* **2011,** *6* (5), 296-301.
19. Kobashi, K.; Villmow, T.; Andres, T.; Pötschke, P., *Sensors and Actuators B: Chemical* **2008,** *134* (2), 787-795.
20. Kazufumi, K.; Tobias, V.; Timo, A.; Liane, H.; Petra, P., *Smart Materials and Structures* **2009,** *18* (3), 035008.
21. Lipomi, D. J.; Vosgueritchian, M.; Tee, B. C. K.; Hellstrom, S. L.; Lee, J. A.; Fox, C. H.; Bao, Z., *Nat Nano* **2011,** *6* (12), 788-792.
22. Zhao, H.; Shen, J.; Zhang, J.; Wang, H.; Wilkinson, D. P.; Gu, C. E., *Journal of Power Sources* **2006,** *159* (1), 626-636.
23. Guo, S.-z.; Yang, X.; Heuzey, M.-C.; Therriault, D., *Nanoscale* **2015,** *7* (15), 6451-6456.
24. Villmow, T.; Pegel, S.; John, A.; Rentenberger, R.; Pötschke, P., *Materials Today* **2011,** *14* (7), 340-345.
25. S. Scott Crump Apparatus and method for creating three-dimensional objects. June, 9, Patent Number 5,121,329**, 1992**.
26. Qin, Z.; Compton, B. G.; Lewis, J. A.; Buehler, M. J., *Nat Commun* **2015,** *6*.
27. Hutmacher, D. W., *Biomaterials* **2000,** *21* (24), 2529-2543.
28. Pham, D. T.; Gault, R. S., *International Journal of Machine Tools and Manufacture* **1998,** *38* (10–11), 1257-1287.
29. Beaman, J. J.; Deckard, C. R. Selective laser sintering with assisted powder handling. **Patent Number 4938816 A,1990**.
30. Jacobs, P. F., *Stereolithography and other RP&M technologies: from rapid prototyping to rapid tooling*. Society of Manufacturing Engineers: **1995**.
31. Zhang, X.; Jiang, X. N.; Sun, C., *Sensors and Actuators A: Physical* **1999,** *77* (2), 149-156.
32. Guo, S.-Z.; Gosselin, F.; Guerin, N.; Lanouette, A.-M.; Heuzey, M.-C.; Therriault, D., *Small* **2013,** *9* (24), 4118-4122.
33. Farahani, R.; Lebel, L.; Therriault, D., *Journal of Micromechanics and Microengineering* **2014,** *24* (5), 055020.

34. Lebel, L. L.; Aissa, B.; Khakani, M. A. E.; Therriault, D., *Advanced Materials* **2010,** *22* (5), 592-596.
35. Ladd, C.; So, J.-H.; Muth, J.; Dickey, M. D., *Advanced Materials* **2013,** *25* (36), 5081-5085.
36. Agarwala, M.; Bourell, D.; Beaman, J.; Marcus, H.; Barlow, J., *Rapid Prototyping Journal* **1995,** *1* (1), 26-36.
37. Leigh, S. J.; Bradley, R. J.; Purssell, C. P.; Billson, D. R.; Hutchins, D. A., *Plos one* **2012,** *7(11)*.
38. Farahani, R. D.; Chizari, K.; Therriault, D., *Nanoscale* **2014,** *6* (18), 10470-10485.
39. Postiglione, G.; Natale, G.; Griffini, G.; Levi, M.; Turri, S., *Composites Part A: Applied Science and Manufacturing* **2015,** *76* (0), 110-114.
40. Zhu, C.; Han, T. Y.-J.; Duoss, E. B.; Golobic, A. M.; Kuntz, J. D.; Spadaccini, C. M.; Worsley, M. A., *Nature communications* **2015,** *6*.
41. Czyżewski, J.; Burzyński, P.; Gaweł, K.; Meisner, J., *Journal of Materials Processing Technology* **2009,** *209* (12–13), 5281-5285.
42. Guo, S.-Z.; Heuzey, M.-C.; Therriault, D., *Langmuir* **2014,** *30* (4), 1142-1150.
43. Chizari, K.; Therriault, D. In *Fabrication of Conductive Microfilaments and Liquid Sensor from CNTs/PLA Nanocomposites*, Design, Manufacturing and Applications of Composites Tenth Workshop 2014: Proceedings of the Tenth Joint Canada-Japan Workshop on Composites, August 2014, Vancouver, Canada, DEStech Publications, Inc: **2015**; p 214.
44. Guo, S. Z.; Gosselin, F.; Guerin, N.; Lanouette, A. M.; Heuzey, M. C.; Therriault, D., *Small* **2013,** *9* (24), 4118-4122.

Figures

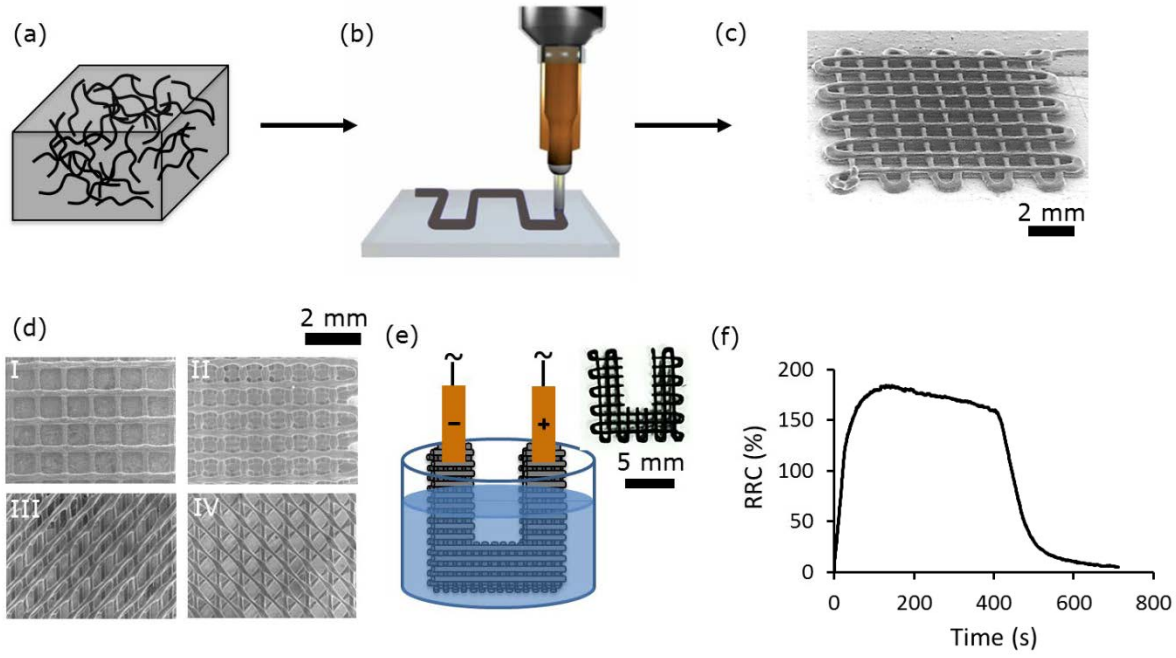

Figure 1. Schematics and SEM images showing the fabrication, the configurations and liquid sensitivity tests of conductive scaffold structures. (a) Schematic of CNT/PLA composites fabricated via ball mill mixing method. (b) Schematics of 3D printing method used for fabrication of CNT/PLA scaffold structures. (c) SEM image of a scaffold printed in two layers using the 3D printing method (d) Top view of SEM images of scaffolds printed in four layers with different patterns. I: Open window, II: Closed window, III: Zigzag I, IV: Zigzag II. (e) Schematic showing liquid sensitivity testing of U shaped cut scaffold. The immersion/drying cycles was 120/600 s. The inset shows a top view optical image of a U shaped cut scaffold (f) A typical liquid sensitivity test graph showing the increase and decrease of the RRC of a liquid sensor while immersion/drying cycles. This

test was on a scaffold with IFS of ~ 0.7, thickness of ~ 0.4 mm and filament diameter of ~231 µm printed in open window pattern.

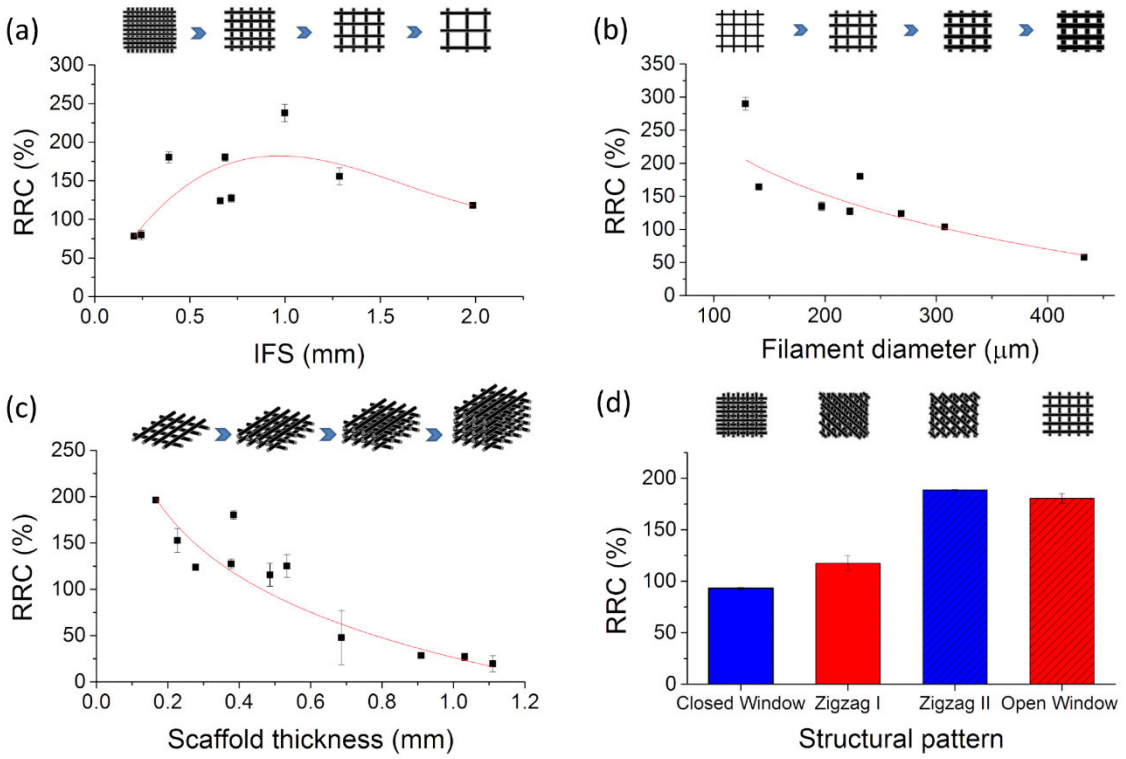

Figure 2. The effect of (a) IFS, (b) filament diameter, (c) scaffold thickness and (d) structure patterns on the liquid sensitivity of the conductive scaffolds. Higher RRC values indicates greater sensitivity of the liquid sensors since they show higher electrical resistance variation when immersed in the testing liquid. The schematics on top of the graphs and the fitted curves are illustrated to facilitate the following of the trend of variables and RRC values, respectively.

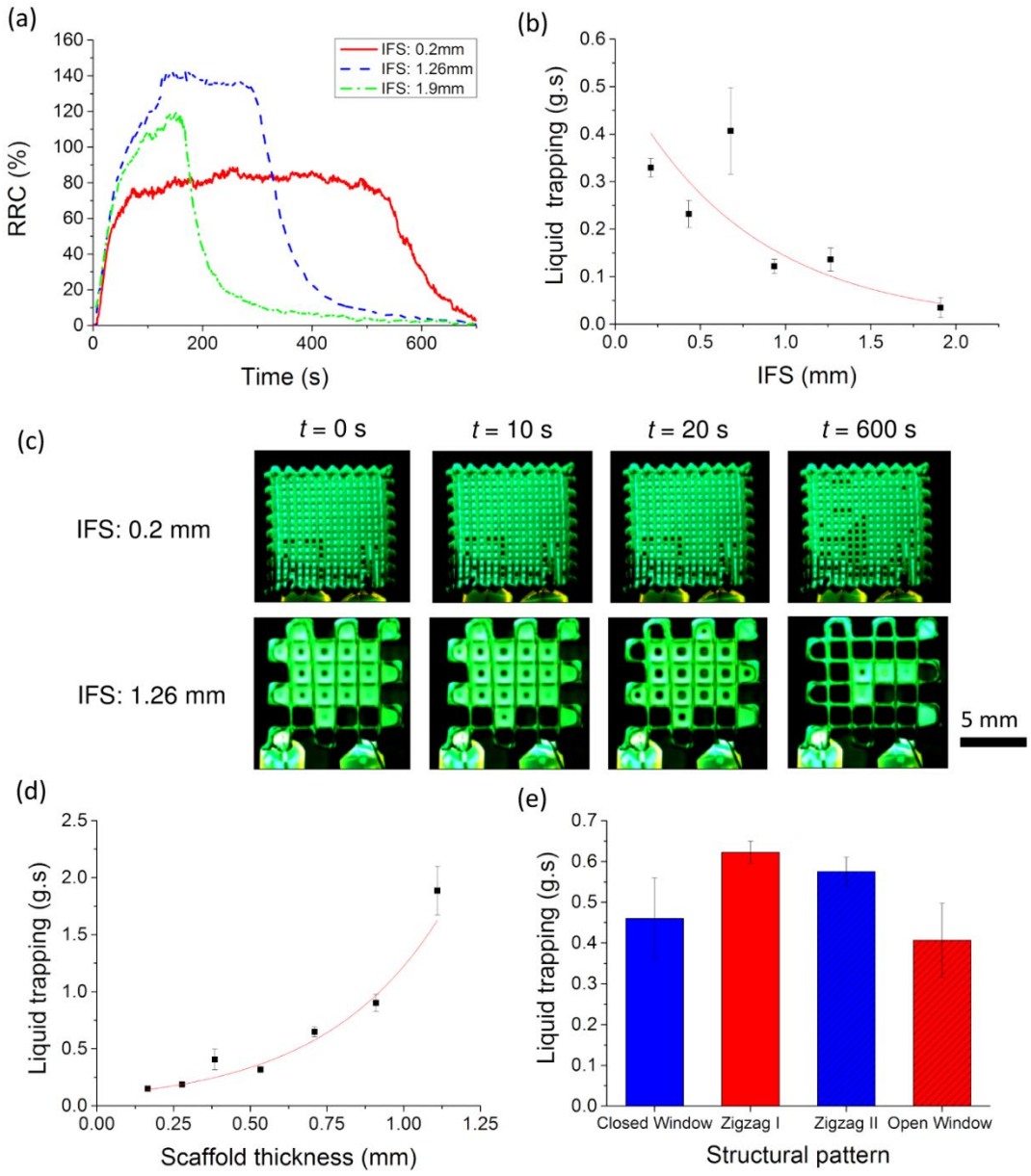

Figure 3. (a) RRC as a function of time during an immersion/drying cycle showing decrease of the RRC peaks width by increasing the IFS indicating longer sensing duration. (b) The variation of liquid trapping during the drying time as a function of IFS. (c) Fluorescent images of scaffolds immersed in a fluorescent liquid under UV lamp showing the escaping of liquid from the structure by time. The scaffold with IFS of 0.2 mm could

keep > 70 % of the initial absorbed liquid during ten minutes while this value was < 30 % for the scaffold with 1.26 mm IFS. Graphs of liquid trapping as a function of (d) scaffold thickness and (e) structure patterns. The influence of IFS and scaffold thickness were more significant compared to the structure patterns. The values of liquid trapping indicate the amount of absorbed liquid that escaped from the scaffold structures over time.

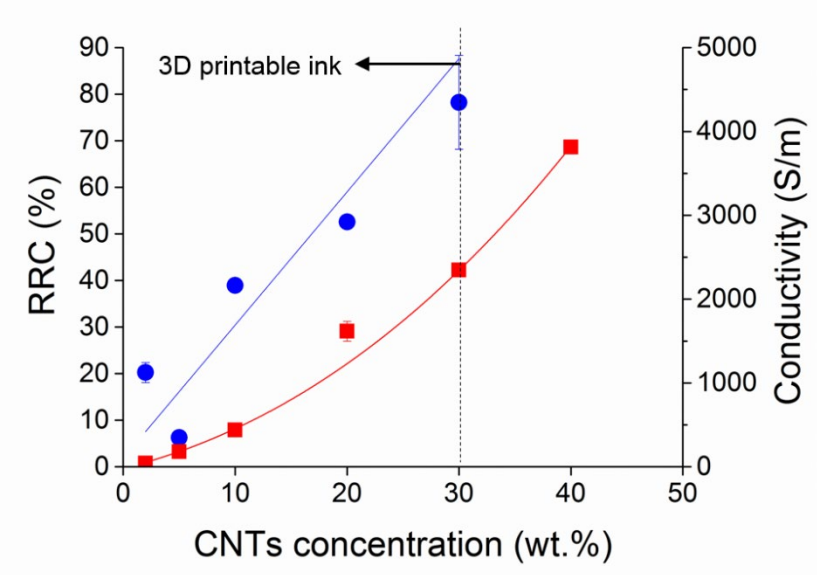

Figure 4. Liquid sensitivity of CNT/PLA scaffolds (●) and electrical conductivity (▪) of bulk CNT/PLA composites as a function of CNTs concentration. The zone before the vertical line is the zone that the CNT/PLA ink can be used for 3D printing by SC3DP method. The liquid sensitivity tests were performed with applied voltage of 1.5 V. Higher liquid sensitivity was obtained for the liquid sensors with higher electrical conductivities.

Supporting Information

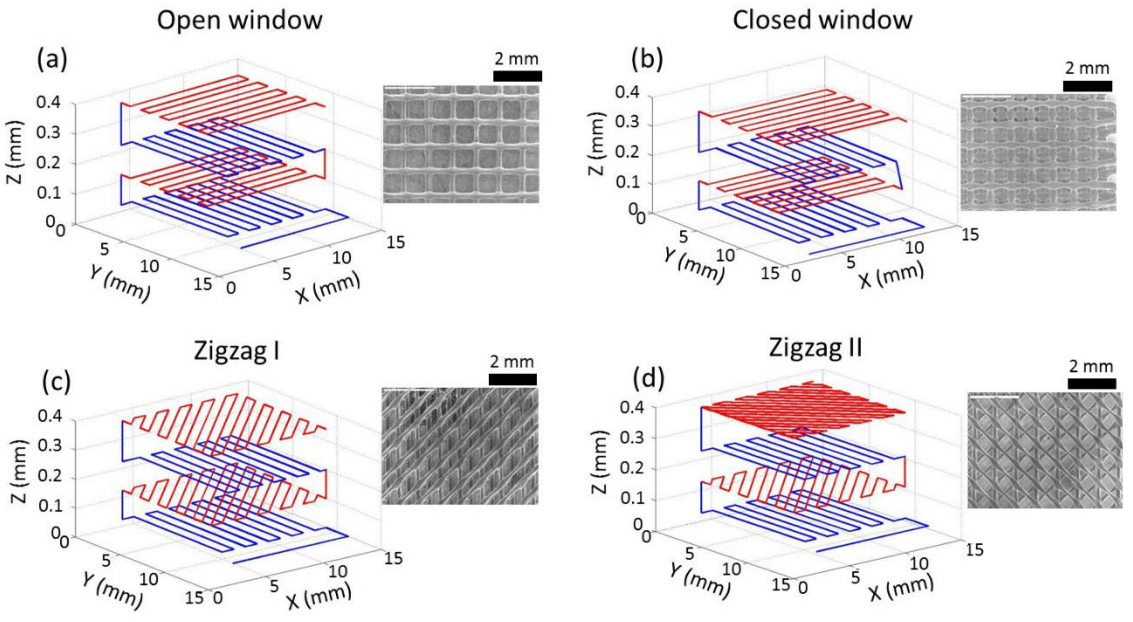

Figure S1. The printing patterns used for fabrication of (a) open window, (b) closed window, (c) Zigzag I and (d) Zigzag II configurations. The third and fourth layers in closed window configuration is placed in between first and second layers in a way that they close the windows formed from printing of the first two layers. The insets are the SEM images of each structure.

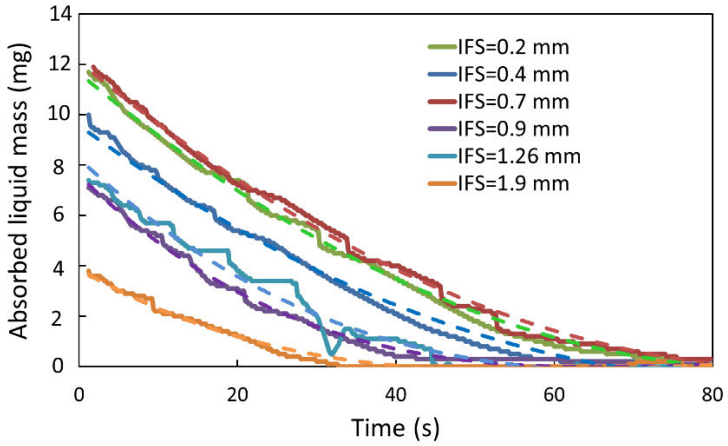

Figure S2. The graphs of mass of absorbed liquid as a function of drying time showing how the mass of the liquid decreased over time. The values of the liquid trapping were calculated from the surface under each graph.